Int. J. Electrochem. Sci., 17 **(2022)** Article Number: 221299, doi: 10.20964/2022.12.110

International Journal of
ELECTROCHEMICAL
SCIENCE
www.electrochemsci.org

Corrosion Inhibition Effect of 2-Chloro-1-(4-fluorobenzyl) benzimidazole on Copper in 0.5 M H_2SO_4 solution

Qingshan Liu[1,*], *Wenwen Xiao*[1], *Pengli Ge*[1], *Wu Long*[1], *Sizhe Gao*[1], *Xiaotong Liu*[2], *Yingfeng Chen*[2]

[1] SINOPEC Northwest Company of China Petroleum and Chemical Corporation, Urumqi 830011, China
[2] Safetech Research Institute (Beijing) Co., Ltd., Beijing, 102209, China
[*]E-mail: 276404102@qq.com

Received: 6 September 2022 / *Accepted:* 21 October 2022 / *Published:* 27 December 2022

2-Chloro-1-(4-fluorobenzyl)benzimidazole (CFB) is the primary intermediate in synthesizing the antiallergic drug mizolastine. In this work, we selected CFB as a candidate to replace toxic and difficult to synthesize inhibitors. Combining electrochemical experiments and Density Functional Theory (DFT) calculations, the anti-corrosion ability of CFB for copper in 0.5 M H_2SO_4 was explored in detail. The electrochemical test indicated that CFB was an excellent inhibitor, which could slow down copper anodic and cathodic dissolution rates. The highest η value reached 95.2% when CFB was 10 mM. Langmuir adsorption isotherm demonstrated that CFB molecules adsorbed to the copper surface by physicochemical action. DFT calculations revealed that the benzene and imidazole rings in CFB were the active sites for adsorption. We believe this work can accumulate experience for developing drug corrosion inhibitors and promote their practical application in the industry.

Keywords: Copper, Corrosion inhibitor, Drug, Electrochemistry, DFT calculation

1. INTRODUCTION

Copper is standard for making cables, electrical, electronic components, and building materials [1, 2]. Copper is also known as “industrial gold” because of its good ductility, electrical conductivity, thermal conductivity, and low cost compared to precious metals [3]. Similar to steel products, copper components can also corrode in service environments. Unlike steel, the corrosion of copper is mainly dominated by oxygen absorption corrosion [4]. Eventually, the copper (Cu^0) is converted to cuprous oxide (Cu_2O), copper oxide (CuO), and verdigris ($Cu_2(OH)_2CO_3$), which are collectively referred to as patina. Pickling is one of the more mature used rust removal methods [5, 6]. Commonly used copper pickling solutions include sulfuric acid, nitric acid, hydrochloric acid, phosphoric acid, oxalic acid, and

mixtures [7, 8]. However, acid can corrode the copper matrix during the pickling process, which is a wasteful and a safety hazard. Corrosion inhibitors are used as additives to slow copper corrosion in the pickling process due to their low dosage and high efficiency [9].

Now recognized corrosion inhibitors are divided into two types, namely inorganic and organic corrosion inhibitors [10]. Inorganics have been widely studied and used in the early stage of corrosion inhibitor development. Unfortunately, researchers found that some inorganic corrosion inhibitors have substantial toxicity, contrary to the current development concept [11]. Therefore, the research, development, and use of organic corrosion inhibitors have been paid more and more attention. Today, many types of organic corrosion inhibitors exist, such as azole derivatives [12], amino acids [13], carbon dots [14], and plant extracts [15]. The corrosion inhibition of 5-Benzyl-1H-Tetrazole (BTA) and 5-(Benzylthio)-1H-tetrazole (BTTA) for copper in a harsh H_2SO_4 solution was comparatively studied by Qiang [16]. Based on EIS and theoretical calculation results, Qiang found that BTTA (99.5%) showed higher protection than BTA (96.1%) because of bridged sulfur atoms in BTTA. Kumar [9] explored the adsorption of Cysteine (CYS), glutamic acid (GLA), glycine (GLY), and their derivative glutathione (GLT) on copper surfaces (111, 100, 110) via DFT calculation. The calculation results such as E_{HOMO} and E_{gap} implied that GLT possessed the highest anti-corrosion ability among four amino acids, which was also proved by Zhang's [17] earlier report. Based on L-serine and citric acid, Zhang [18] synthesized a functional carbon dot by hydrothermal method and studied its corrosion inhibition ability for copper in acid solution. EIS results indicated that 200 mg/L N-CDs exhibited supreme anti-corrosion for copper, even under temperature and time changes. Tan [19] found that Papaya leaves extract (PLE) can act as an eco-friendly corrosion inhibitor for copper. Combining XPS (X-ray Photoelectron Spectroscopy) and adsorption model, Tan also analyzed the anti-corrosion mechanism of PLE for copper in acid.

Organic drugs are well known for their ability to treat various diseases. Drugs may also be effective corrosion inhibitors because they contain heterocycles, heteroatoms, and unsaturated bonds [20]. Besides drug corrosion inhibitors are eco-friendly and less harmful to humans. Li [21] found that losartan potassium (LP, antihypertensive drugs) was an excellent corrosion inhibitor for copper in 0.5 M H_2SO_4. The authors also explain the anti-corrosion mechanism of LP on copper at different temperatures (298 K to 308 K). Nevertheless, much basic research is still needed to promote the practical application of drug corrosion inhibitors, especially to develop more drug corrosion inhibitors.

2-Chloro-1-(4-fluorobenzyl)benzimidazole (CFB) is the primary intermediate in synthesizing the antiallergic drug mizolastine. As shown in Fig. 1, since it contains benzene rings, imidazole rings, and heteroatoms, CFB also has the potential to become a corrosion inhibitor. So far, no work has been dedicated to exploring CFB as an eco-friendly inhibitor for metals in acidic environments. In this work, we fill this vacancy. Based on EIS (Electrochemical Impedance Spectroscopy), PDP (Potentiodynamic Polarization), SEM (Scanning Electron Microscope), LSCM (Laser Scanning Confocal Microscope), and DFT (Density Functional Theory) calculations, the anti-corrosion performance and mechanism of CFB for copper in 0.5 M H_2SO_4 were explored and analyzed in detail. The authors hope this work can accumulate experience for developing drug corrosion inhibitors and promote their practical application in industry.

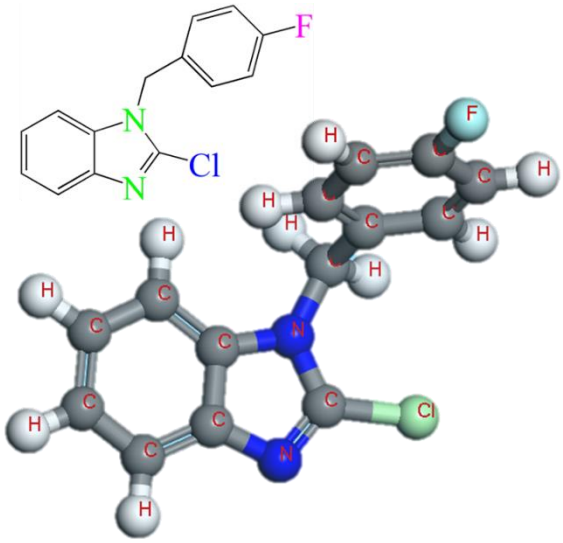

Figure 1. The chemical structure of CFB.

2. EXPERIMENTAL

2.1 materials

Pure copper (99.9%) was purchased from the center of Shengxin Corrosion Testing Equipment, China. 2-Chloro-1-(4-fluorobenzyl)benzimidazole (CFB, 97%) and concentrated sulfuric acid (98%) were obtained from Sinopharm Group, China. The copper sample size was 1×1×1 cm^3 and was used without other processing. Other surfaces were sealed by epoxy for the copper electrode, leaving only a 1×1 cm^2 working surface. The electrode was polished with 400 to 2000 mesh sandpaper before electrochemical testing.

The test solution was 0.5 M H_2SO_4, prepared using concentrated sulfuric acid and deionized water. The additive amounts of CFB in the acid solution were 0.5, 1, 3, 5, and 10 mM.

2.2 Electrochemical tests

Based on a traditional three-electrode system, the CHI 660E workstation finished all electrochemical tests in this work. Here, copper (1 cm^2), platinum sheet (4 cm^2), and saturated calomel electrode were the working, counter, and reference electrodes. After the test system was stabilized, the EIS (Electrochemical Impedance Spectroscopy) experiment was executed. The test range of EIS was 10^5 to 10^{-2} Hz, and the disturbance AC signal was 5 mV. The PDP (Potentiodynamic Polarization) test was carried out when the EIS was finished. The test range of PDP was ±0.25 V vs. self-corrosion potential, and the scanning rate was 1 mV/s. All EIS and PDP tests were executed under a water bath at 298 K.

2.3 Gravimetric measurement

The copper sample was polished with 400 to 2000 mesh sandpaper and was washed with pure water, ethanol, and acetone before the gravimetric test. Then, the sample was immersed in test solutions containing different concentrations of CFB for 48 h. After that, the test sample was washed with pure water, ethanol, and acetone and dried with N_2. Finally, the corrosion rate and anti-corrosion efficiency were calculated from the weight loss of the sample.

2.4 Surface characterization

The copper sample used for SEM (Scanning Electron Microscope) observation was polished with 400 to 7000 mesh sandpaper. Then, the sample was washed with pure water, ethanol, and acetone to remove grease and impurities. After that, the pretreated sample was immersed in test solution containing different concentrations of CFB (0 and 10 mM) for 48 h and repeated the above cleaning process. Finally, the sample was observed by SEM (EVO18, ZEISS).

The copper sample processing procedure for LSCM (Laser Scanning Confocal Microscope) observation was the same as SEM. Then the sample was observed via LSCM (LSCM700, Germany).

2.5 Calculation details

In this work, DFT (Density Functional Theory) calculation was carried out by Materials Studio (MS) software. Based on the B3LYP method within the DFT level with 6 311++G(d, p) basis set, the 3D structure of CFB was optimized [22-24]. Then, the electron cloud distribution of frontier molecular orbital (FMO) and ESP was calculated. Some fundamental quantum chemical parameters were given and discussed detailedly.

3. RESULTS AND DISCUSSION

3.1 EIS

The Nyquist, Bode, and Phase angle plots of copper in 0.5 M H_2SO_4 solution within various concentrations of CFB were given in Fig. 2. As shown in Fig. 2a, the blank EIS curve of copper consisted of an imperfect semicircle and a sloping straight line. The imperfect semicircle was because the experiments were not conducted under ideal conditions, also called the frequency dispersion of interfacial impedance [25]. In addition, the semicircle corresponded to charge transfer and capacitive impedance. That was to say, the larger the semicircle, the larger the impedance value [26]. In other words, the size of the semicircle was positively related to the anti-corrosion of inhibitors. The sloping straight line was called Warburg impedance (W) due to the diffusion of copper ions into the solution and/or the distribution of dissolved oxygen to the copper surface [27]. That was to say, copper was corroded in 0.5 M H_2SO_4, and the phenomenon of ion diffusion further appeared.

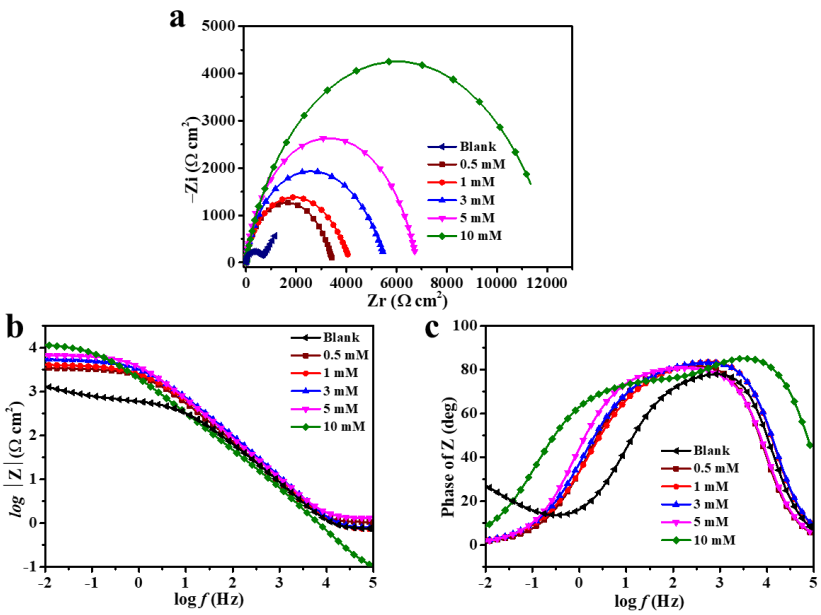

Figure 2. EIS plots of copper in 0.5 M H_2SO_4 solution within various concentrations of CFB.

Fortunately, the presence of CFB increased the radius of the semicircle, and this phenomenon became more pronounced with increasing CFB concentration. At the same time, Warburg impedance also disappeared with the appearance of CFB. These phenomena indicated that CFB improved the copper surface capacitive reactance and charge transfer resistance. Furthermore, the diffusion of copper surface ions was also suppressed by CFB. With enhancing the CFB concentration to 10 mM, the diameter of the semicircle was the biggest, proving that the CFB adsorption film became denser and thus gave a vital inhibitive ability against corrosion media [28].

The related Bode and Phase plots of copper within various concentrations of CFB were displayed in Figs. 2b and c. The impedance modulus of low-frequency significantly enhanced with the appearance of CFB and the addition of concentration. Compared with the blank and 10 mM, it was noted that the low-frequency impedance modulus value of copper in acid solution increased by an order of magnitude. This finding indicated that a high-efficiency adsorption film was formed on the copper surface, which blocked the contact between the corrosive media and the copper surface [29]. The change in the frequency range corresponding to the max value in the Phase angle diagram also proved this result. It was worth noting that there were two max values in the Phase angle plot, which correspond to two-time constants.

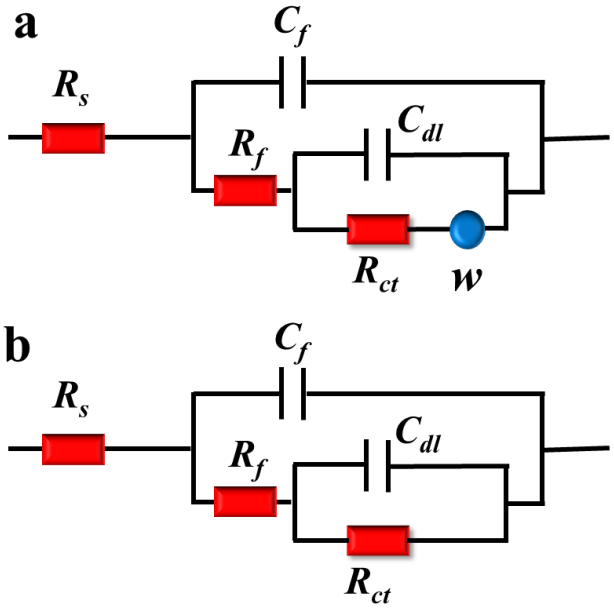

Figure 3. The relevant equivalent circuits used in this work.

To gain a more accurate understanding of the effect of CFB on the copper surface, we fitted the EIS data. The relevant equivalent circuits used in this work were given in Fig. 3. Here, R_s, R_f, and R_{ct} were the solution, film, and charge transfer impedance, while C_{dl} and C_f were the double-layer and film capacitance. All electrochemical parameters were displayed in Table 1. As shown in Table 1, the R_f and R_{ct} value of copper was enhanced when CFB appeared in the acid solution. The values of R_f and R_{ct} reached 391 and 12310 Ω cm^2 when the concentration of CFB was 10 mM.

On the contrary, the values of C_{dl} and C_f were reduced to 4.5 and 18.9 μF cm^{-2}, respectively. It was proved that CFB could adsorb on the copper surface and form a dense protective film. There was no doubt that CFB molecules were more dominant in the competitive adsorption with H_3O^+ and Cl^- ions, which was beneficial for forming a CFB shielding film on the copper surface. Based on the work of other researchers [30], the inhibition efficiency (η) was calculated and also given in Table 1. The highest η value was 95.2% when CFB concentration reached 10 mM, which also corresponded to the supreme anti-corrosion.

Table 1. Some EIS parameters of copper within various concentrations of CFB.

C (mM)	R_f (Ω cm^2)	R_{ct} (Ω cm^2)	C_f (μF cm^{-2})	n_1	C_{dl} (μF cm^{-2})	n_2	W (×10^{-2}Ω cm^2 $s^{1/2}$)	η (%)
Blank	38	570	47.5	1	86.2	0.67	4.61	-
0.5	58	3413	18.1	1	48.3	0.65	-	82.5
1	111	4066	15.3	1	40.1	0.60	-	85.4
3	194	5400	13.1	1	34.1	0.63	-	89.1
5	243	6574	10.2	1	30.0	0.73	-	91.1
10	391	12310	4.5	1	18.9	0.72	-	95.2

3.2 PDP

The Potentiodynamic polarization curve of copper in 0.5 M H_2SO_4 solution within various concentrations of CFB was given in Fig. 3. It can be seen in Fig. 3 that the anodic and cathodic branches of copper PDP were shifted down when CFB was added in 0.5 M H_2SO_4. This phenomenon was more pronounced when CFB was 10 mM. These results indicated that CFB could significantly reduce the cathodic and anodic reactions on the copper surface and provide comprehensive protection for copper. A platform was observed between -0.07 V to 0.03 V in 10 mM PDP, which was attributed to the slowest desorption of CFB molecules from the copper surface [31]. This finding further demonstrated the highest shielding performance of 10 mM CFB against copper. Comparing all PDP curves, they held a similar shape, which indicated that the presence of CFB did not change the reaction mechanism of copper in the acidic environment [32].

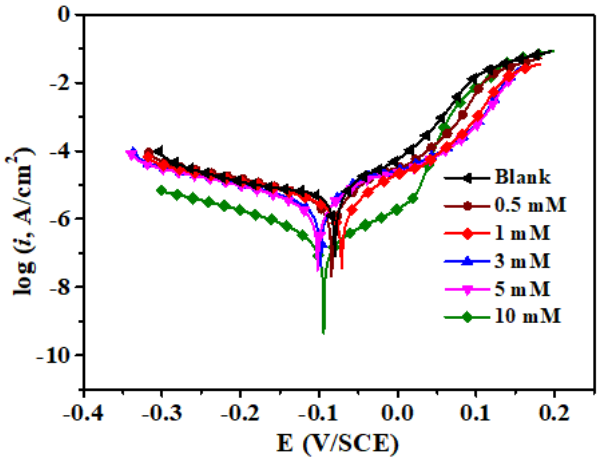

Figure 4. PDP plots of copper in 0.5 M H_2SO_4 solution within various concentrations of CFB.

Some key PDP parameters were obtained based on extrapolation, such as E_{corr}, i_{corr}, cathodic (β_c), and anodic slopes (β_a). Based on the work of other researchers, the inhibition efficiency (η) was calculated and given in Table 2 [33]. As shown in Table 2, the value change of E_{corr} was no more than 80 mV, indicating that CFB was a modest and mixed-type inhibitor for copper. The blank i_{corr} value was 65.7 μA cm^{-2}, while the i_{corr} value of 0.5 mM CFB was 13.1 μA cm^{-2}, which indicated that CFB could significantly slow down the conversion rate of copper atoms (Cu^0) into copper ions (Cu^+, Cu^{2+}). As the concentration of CFB increased to 10 mM, the i_{corr} value decreased to 4.1 μA cm^{-2}. In this situation, an active shielding effect can be deduced from fabricating an anchored CFB-adsorption layer on the copper surface, which can provide a satisfactory protective shield against acid media attacks. At the same time, the η value increased with the augment of CFB concentration and was always kept at an excellent level. Specifically, the highest η value was 93.8%, which proved that CFB could afford an incredible anti-corrosion performance for copper in 0.5 M H_2SO_4.

Table 2. Some PDP parameters of copper within different concentrations of CFB.

C (mM)	E_{corr} (mV/SCE)	I_{corr} (μA cm^{-2})	β_c (mV dec^{-1})	β_a (mV dec^{-1})	η (%)
Blank	–80	65.7	–261	56	–
0.5	–84	13.1	–221	70	80.0
1	–71	10.8	–205	72	83.5
3	–98	9.1	–248	65	86.1
5	–102	7.1	–233	67	89.2
10	–94	4.1	–212	75	93.8

3.3 Gravimetric measurement

The dissolution rate of copper in 0.5 M H_2SO_4 within various CFB concentrations was given in Fig. 5a. There was no doubt that the dissolution rate of copper in the blank acidic solution was the highest and attained 230.5 mg m^{-2} h^{-1}, which proved that copper was stiff to withstand acid corrosion. With the advent of CFB, the dissolution rate of copper dropped by an order of magnitude, which was 42.6 mg m^{-2} h^{-1}. When CFB was raised to 10 mM, the dissolution rate of copper decreased to the lowest, only 14.3 mg m^{-2} h^{-1}. Conversely, the value of η enhanced with the concentration of CFB, and the highest η value was 93.8% in Fig. 5b. Gravimetric measurement results were consistent with the electrochemical tests, which demonstrated the indispensable protection capability of CFB for copper.

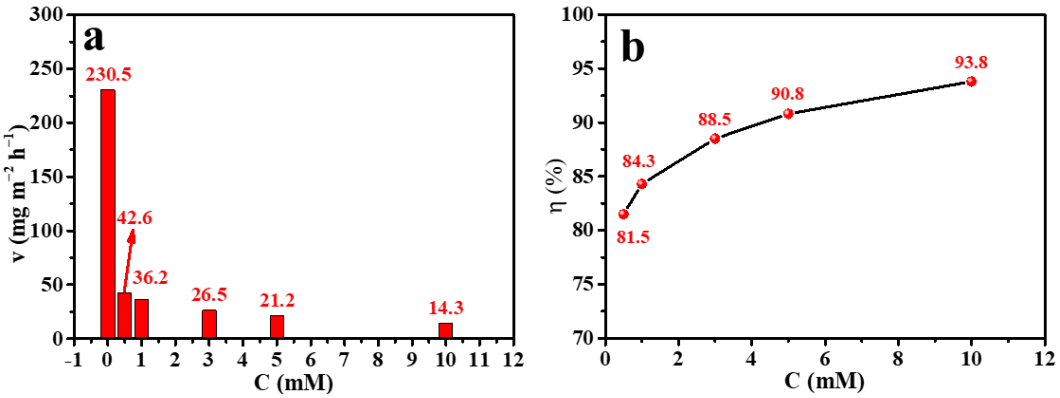

Figure 5. The change of dissolution rate and inhibition ability of copper in 0.5 M H_2SO_4 containing various concentrations of CFB.

3.4 Corrosion morphology

The flat and tridimensional corrosion morphology of copper with 0 and 10 mM CFE acidic solution was displayed in Figs. 6 and 7. As distinctly seen the copper surface (Fig. 6a) in the absence of CFB was severely eroded, and many rough corrosion products appeared. At the same time, it was hard to observe a neat and smooth copper surface in Fig. 6a. Interestingly, CFB protected copper substrate

was flat and smooth, demonstrating that a CFB film was assembled on the copper surface. Some inevitable pitting corrosion still appeared on the copper substrate under the protection of CFB, which implied that the CFB film could not entirely cut off the contact between the corrosion ions and the copper substrate.

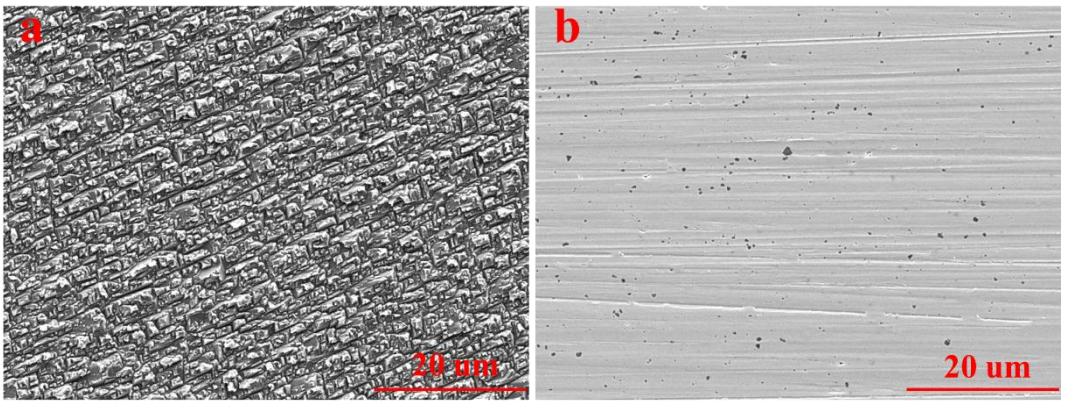

Figure 6. SEM images of the copper matrix after immersing in 0.5 M H_2SO_4 without (a) and with 10 mM (b) CFB.

It could noted that without CFB protected copper surface was accumulated many raised and rough corrosion products in Fig. 7a. The corroded copper surface was no longer smooth, like a group of hills. Compared with Fig. 7a, CFB protected copper surface was flat and smooth, and corrosion products were hardly seen. It was further noticed that the R_a value of 10 mM CFB was 0.12 um while the R_a value of blank was 1.35 um, showing that the dense CFB film could provide excellent protection for copper.

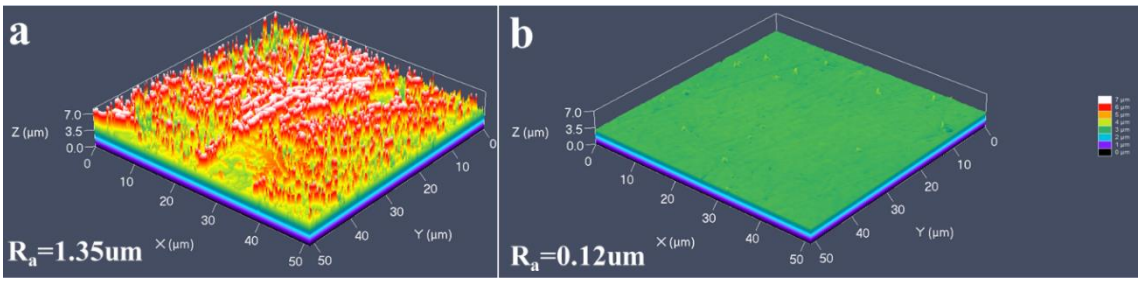

Figure 7. LSCM images of the copper matrix after immersing in 0.5 M H_2SO_4 without (a) and with 10 mM (b) CFB.

.

3.5 Adsorption isotherm

Adsorption isotherm was used to investigate the assembly mechanism of CFB film at the copper/corrosion medium interface. The EIS data were used to fit the Langmuir adsorption isotherm. It

could be seen in Fig. 8 that the goodness of fit value (R^2) was 0.9997 (close to1), implying that the CFB molecules' adsorption on the copper surface belonged to the Langmuir adsorption isotherm. Based on current work, it could be inferred that all CFB molecules and corrosive ions (H_3O^+, Cl^-) held an equal chance when adsorbed on the copper surface. Combining the electrochemical results, it can be found that CFB molecules replace a large number of corrosive ions and form a protective film. To further estimate the adsorption type of CFB molecules on the copper surface, some thermodynamic parameters were calculated via Eqs. 1 and 2 [34].

$$\frac{C}{\theta}=\frac{1}{K_{ads}}+C \quad (1)$$

$$K_{ads}=\frac{1}{1000}\exp(-\frac{\Delta G^0_{ads}}{RT}) \quad (2)$$

The obtained thermodynamic parameters were given in Fig. 8. Quite frankly, the high K_{ads} value stood for the excellent adsorption ability of the inhibitor. In this work, CFB possessed a higher K_{ads} value (96.0 10^3 L/mol), which meant that CFB molecules could quickly adsorb to the copper surface and form a dense protective film [35]. Generally speaking, the adsorption type was chemical when ΔG^0_{ads} value was less than -40 kJ/mol, while it was physical when ΔG^0_{ads} value exceeded -20 kJ/mol. In this work, the ΔG^0_{ads} value was 38.4 kJ/mol, between -20 and -40 kJ/mol, indicating that the adsorption of CFB molecules on the copper surface was a joint action of physicochemical. It was worth noting that chemisorption played a dominant role in the whole adsorption process.

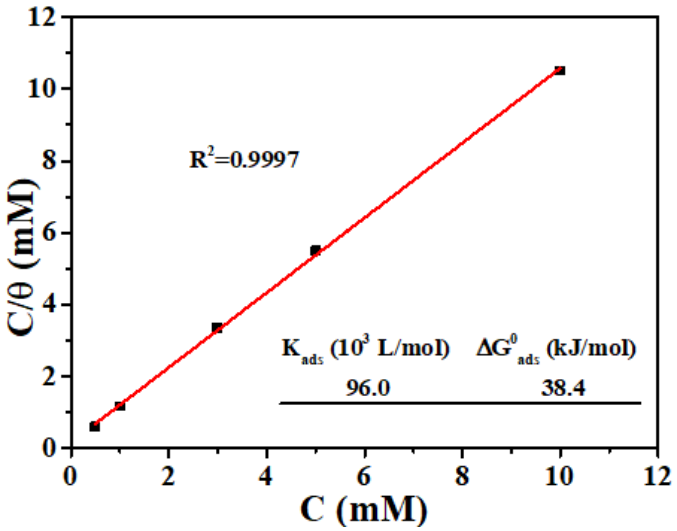

Figure 8. Langmuir adsorption isotherm and thermodynamic parameters fitted by EIS results.

3.6 computational details

DFT calculation was employed to explore the correlation between organic molecular structure and inhibitory properties. The optimized structure, FMO distributions, and ESP of CFB were displayed in Fig. 9. It could be seen in the optimized structure (Fig. 9a) that a benzene ring and imidazole rings were in the same plane, while the other benzene ring was twisted. This phenomenon could be attributed to the steric hindrance inside the CFB molecule, implying that the CFB molecule was easily polarized.

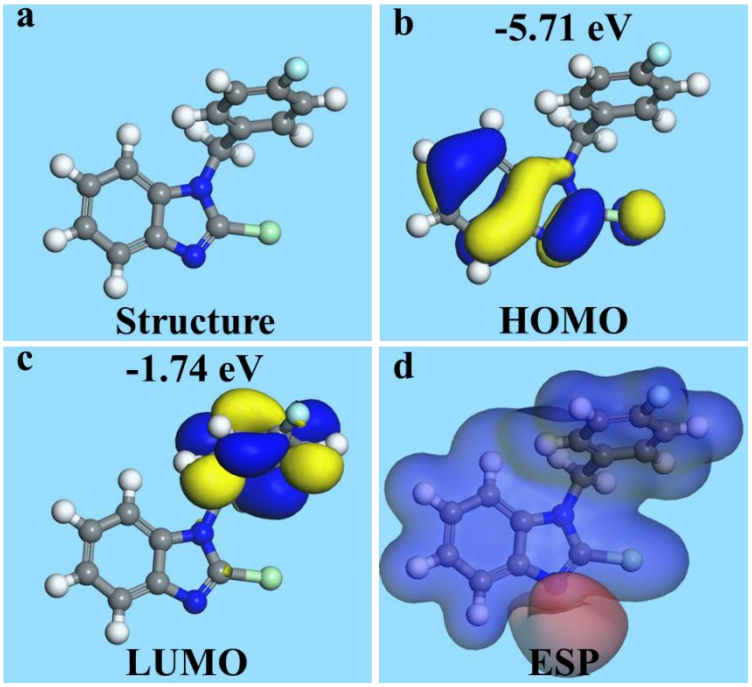

Figure 9. The structure (a), FMO distributions (b-c), and ESP (d) of CFB.

As was well known, FMO distributions included the highest occupied molecular orbital (HOMO) and lowest unoccupied molecular orbital (LUMO). Here, HOMO stood for offer electronics ability of inhibitor, while LUMO was the performance to obtain electronics [36]. It was seen the HOMO electronic cloud was located on the benzene ring and imidazole rings of CFB. The LUMO electronic cloud was distributed on another benzene ring. In general, FMO electronic cloud occupied the entire CFB molecule, which was beneficial for CFB molecules to adsorb on the copper surface by gaining and losing electrons. This result was also consistent with the distribution of electrophilic activity (blue) and nucleophilic activity (red) in ESP (Fig. 9d).

Besides, ΔE (ΔE=E_{LUMO}-E_{HOMO}) and dipole moment (m) were calculated and analyzed in detail. Based on E_{LUMO} (-1.74 eV) and E_{HOMO} (-5.71 eV), ΔE was obtained (3.97 eV). It was worth noting that the value of ΔE was lower in this work, which indicated the higher adsorption activity of CFB molecules for copper [37]. Dipole moment (m) represented mutually exclusive capabilities between organic molecules. A small m value corresponds to the weak mutual repulsion between molecules [38]. A lower m value (6.72 D) was gained in this work, which implied that a large number of CFB molecules could accumulate on the copper surface and form a dense film. All in all, the DFT calculation disclosed the adsorption mechanism of CFB molecules on the copper surface from the molecular level.

4. CONCLUSION

Combining experiments and DFT calculations, the anti-corrosion performance of 2-Chloro-1-(4-fluorobenzyl)benzimidazole (CFB) for copper in 0.5 M H_2SO_4 was explored. Some main results were concluded as follows.

1. EIS results indicated that CFB could effectively inhibit the corrosion rate of copper in acidic medium and enhance copper charge transfer and film impedance. The η value was enhanced with the increase in CFB concentrations, and the highest η value was 95.2%.

2. Based on PDP tests, it was found that CFB was a modest and mixed-type inhibitor for copper. Besides, CFB could inhibit the anodic and cathodic reactions of copper. Gravimetric measurements showed that CFB reduced the dissolution rate of copper, especially the concentration of CFB was increased to 10 mM.

3. SEM and LSM plots revealed that a CFB film was fabricated on the copper surface, blocking the connection between the copper and the corrosive medium. The copper surface became more flat and smooth under the CFB protection. These results are consistent with the above electrochemical results.

4. The Langmuir adsorption model found that the adsorption type of CFB was a joint action of physicochemical, and chemisorption played a dominant role. Combined with DFT calculations, it was discovered that CFB molecules adsorbed on the copper surface through the benzene ring and imidazole ring in parallel, which disclosed the adsorption mechanism of CFB molecules from the molecular level.

References

1. Y. Qiang, S. Zhang, S. Xu, and W. Li, *Journal of Colloid and Interface Science,* 472 (2016) 52-59.
2. Y. Qiang, S. Zhang, H. Zhao, B. Tan, and L. Wang, *Corrosion Science,* 161 (2019) 108193.
3. Y. Wu, W. Zhao, Z. Lu, and L. Wang, *Carbon,* 179 (2021) 445-457.
4. Y. Wu, T.Y. Sun, T. Ge, W. Zhao, and L.F. Huang, *Advanced Functional Materials,* 32 (2021) 2110264.
5. S. Eid, *International Journal of Electrochemical Science,* 16 (2021) 150852.
6. H. A. Alrafai, *International Journal of Electrochemical Science,* 17 (2022) 220216.
7. H. Li, S.T. Zhang, and Y.J. Qiang, *Journal of Molecular Liquids,* 321 (2021) 114450.
8. Y. Qiang, S. Zhang, and L. Wang, *Applied Surface Science,* 492 (2019) 228-238.
9. D. Kumar, N. Jain, V. Jain, and B. Rai, *Applied Surface Science,* 514 (2020) 145905.
10. P.E. Alvarez, M.V. Fiori-Bimbi, A. Neske, S.A. Brandán, and C.A. Gervasi, *Journal of Industrial and Engineering Chemistry,* 58 (2018) 92-99.
11. D.A. Winkler, M. Breedon, P. White, A.E. Hughes, E.D. Sapper, and I. Cole, *Corrosion Science,* 106 (2016) 229-235.
12. Y. Qiang, H. Zhi, L. Guo, A. Fu, T. Xiang, and Y. Jin, *Journal of Molecular Liquids,* 351 (2022) 118638.
13. J. Bao, H. Zhang, X. Zhao, and J. Deng, *Chemical Engineering Journal,* 341 (2018) 146-156.
14. S. Cao, D. Liu, T. Wang, A. Ma, C. Liu, X. Zhuang, H. Ding, B.B. Mamba, and J. Gui, *Colloids and Surfaces A: Physicochemical and Engineering Aspects,* 616 (2021) 126280.
15. H. Li, Y.J. Qiang, W.J. Zhao, and S.T. Zhang, *Colloids and Surfaces a-Physicochemical and Engineering Aspects,* 616 (2021) 126077.
16. Y. Qiang, H. Li, and X. Lan, *Journal of Materials Science & Technology,* 52 (2020) 63-71.
17. D.-Q. Zhang, B. Xie, L.-X. Gao, Q.-R. Cai, H.G. Joo, and K.Y. Lee, *Thin Solid Films,* 520 (2011) 356-361.
18. Y. Zhang, S. Zhang, B. Tan, L. Guo, and H. Li, *Journal of Colloid and Interface Science,* 604 (2021) 1-14.
19. B. Tan, B. Xiang, S. Zhang, Y. Qiang, L. Xu, S. Chen, and J. He, *Journal of Colloid and Interface Science,* 582 (2021) 918-931.
20. Y. Qiang, L. Guo, H. Li, and X. Lan, *Chemical Engineering Journal,* 406 (2021) 126863.
21. H. Li, S. Zhang, B. Tan, Y. Qiang, W. Li, S. Chen, and L. Guo, *Journal of Molecular Liquids,* 305

(2020) 112789.
22. W. Chen, and W.W. Xiao, *International Journal of Electrochemical Science*, 17 (2022) 220427.
23. A. Dehghani, G. Bahlakeh, B. Ramezanzadeh, A. Hossein Jafari Mofidabadi, and A. Hossein Mostafatabar, *Journal of Colloid and Interface Science*, 603 (2021) 716-727.
24. M.H. Shahini, M. Keramatinia, M. Ramezanzadeh, B. Ramezanzadeh, and G. Bahlakeh, *Journal of Molecular Liquids*, 342 (2021) 117570.
25. Y. Qiang, S. Fu, S. Zhang, S. Chen, and X. Zou, *Corrosion Science*, 140 (2018) 111-121.
26. Y.X. Liu, X.Q. Yao, C.L. Liu, X.F. Luo, C. Guo, and W. Du, *International Journal of Electrochemical Science*, 17 (2022) 220445.
27. B. Tan, S. Zhang, Y. Qiang, L. Guo, L. Feng, C. Liao, Y. Xu, and S. Chen, *Journal of Colloid and Interface Science*, 526 (2018) 268-280.
28. H. Li, Y. Qiang, W. Zhao, and S. Zhang, *Corrosion Science*, 191 (2021) 109715.
29. M. Ramezanzadeh, G. Bahlakeh, Z. Sanaei, and B. Ramezanzadeh, *Applied Surface Science*, 463 (2019) 1058-1077.
30. P.C. Okafor, M.E. Ikpi, I.E. Uwah, E.E. Ebenso, U.J. Ekpe, and S.A. Umoren, *Corrosion Science*, 50 (2008) 2310-2317.
31. J. He, Q. Li, X. Li, J. An, G. Chen, L. Zhao, and W. Li, *Journal of Molecular Liquids*, 320 (2020) 114494.
32. Q. Zhang, P. Liu, Z. Zhu, J. Zhang, and F. Cao, *Corrosion Science*, 164 (2020) 108312.
33. J. Haque, V. Srivastava, M.A. Quraishi, D. Singh Chauhan, H. Lgaz, and I.-M. Chung, *Corrosion Science*, 172 (2020) 108665.
34. M. Oubaaqa, M. Ouakki, M. Rbaa, A.S. Abousalem, M. Maatallah, F. Benhiba, A. Jarid, M. Ebn Touhami, and A. Zarrouk, *Journal of Molecular Liquids*, 334 (2021) 116520.
35. X. Yao, Y. Qiang, L. Guo, Q. Xu, L. Wen, and Y. Jin, *Journal of Industrial and Engineering Chemistry*, 114 (2022) 427-437.
36. E. Alibakhshi, M. Ramezanzadeh, S.A. Haddadi, G. Bahlakeh, B. Ramezanzadeh, and M. Mahdavian, *Journal of Cleaner Production*, 210 (2019) 660-672.
37. Y. Yan, W. Li, L. Cai, and B. Hou, *Electrochimica Acta*, 53 (2008) 5953-5960.
38. H.M. Abd El-Lateef, *Applied Surface Science*, 501 (2020) 144237